VERIFICATION OF THE AWA PHOTOINJECTOR BEAM PARAMETERS REQUIRED FOR A TRANSVERSE-TO-LONGITUDINAL EMITTANCE EXCHANGE EXPERIMENT

M. M. Rihaoui[1,2], P. Piot[1,3], J. G. Power[2], D. Mihalcea[1], and W. Gai[2]
[1] Department of Physics, Northern Illinois University DeKalb, IL 60115
[2] High Energy Physics Division, Argonne National Laboratory, Argonne, IL 60439, USA
[3] Accelerator Physics Center, Fermi National Accelerator Laboratory, Batavia, IL 60510, USA*

Abstract

A transverse-to-longitudinal emittance exchange experiment is in preparation at the Argonne Wakefield Accelerator (AWA). The experiment aims at exchanging a low ($\varepsilon_z < 5$ μm) longitudinal emittance with a large ($\varepsilon_x > 15$ μm) transverse horizontal emittance for a bunch charge of ~ 100 pC. Achieving such initial emittance partitioning, though demonstrated via numerical simulations, is a challenging task and needs to be experimentally verified. In this paper, we report preliminary emittance measurements of the beam in the transverse and longitudinal planes performed at ~ 12 MeV. The measurements are compared with numerical simulations.

INTRODUCTION

Plans are underway at the Argonne Wakefield Accelerator (AWA) [1] to perform a proof-of-principle experiment aim at demonstrating the exchange of a large transverse emittance with a lower longitudinal one. The emittance exchange concept could have application in $e+/e-$ linear collider where its implementation could eventually eliminate the need for an electron damping ring. The technique could also be beneficial to single-pass high-gain FELs where the reduction of the transverse emittance at the expense of an increased longitudinal emittance could improve the gain length while simultaneously mitigating microbunching effects.

The layout of the proof-of-principle experiment is presented in Fig. 1. In brief, electron bunches with charge of $Q = 100$ pC are generated via photo-emission from a magnesium photocathode located at the back plate of a 1-1/2 cell rf gun operating at 1.3 GHz. The rf gun is surrounded by three solenoidal lenses (labeled L1, L2, and L3 in Fig. 1) used to control the beam transverse size. The beam is then accelerated to 12 MeV using a 1.3 GHz standing wave structure (refer to as booster) operating on the $\mathrm{TM}_{010,\pi/2}$ mode. The downstream beamline incorporates four quadrupoles followed by the emittance exchanger beamline. The latter beamline, designed to swap the horizontal (x, x') and longitudinal (z, δ) phase spaces, consists of a horizontally-deflecting cavity, operating on the TM_{110} mode, flanked by two identical horizontally-dispersive sections henceforth refereed to as "dogleg."

In the present configuration the exchanger is not installed and the beamline downstream of the booster includes three quadrupoles arranged as a triplet followed by a spectrometer. The beamline also incorporates YAG:Ce screens for measuring the beam's transverse density. One of these screens is located in the spectrometer line at a large vertical dispersion point.

During nominal operation, the AWA is tuned to minimize the transverse emittance with no particular attention to the longitudinal emittance. The proof-of-principle experiment discussed in the Paper requires a different mode of operation where the longitudinal emittance is made smaller than the transverse one by a factor ~ 3.

NUMERICAL MODELING

We relied on extensive beam dynamics modeling to seek an operating mode of the AWA capable of achieving an emittance partition with $\varepsilon_x/\varepsilon_z > 3$. The program ASTRA [3] along with a multi-objective genetic optimization algorithm [2] were used to find possible operational settings. In these simulations the photocathode drive laser was taken to be transversely uniform with a Gaussian temporal distribution. The variable parameters used for the optimization were the laser pulse duration σ_t, its transverse beam size on the photocathode σ_c, the rf gun phase and peak E-field, the peak B-field associated to the three solenoids surrounding the rf gun, and the booster phase and peak E-field. The optimization was constrained to achieve and emittance ratio $\varepsilon_x/\varepsilon_z > 3$ with $\varepsilon_x < 20$ μm and the longitudinal phase space correlation was required to match a value close to $d\delta/dz|_{z=0} \simeq 8$ m^{-1} to minimize emittance dilution in the exchanger beamline [7].

Astra simulations indicates, for a laser pulse length of $\sigma_t \sim 0.56$ ps, that the achievable emittance partition is $(\varepsilon_x, \varepsilon_z) = (15.9, 3.75)$ μm; see Fig. 2. For the series of measurement reported below the laser pulse length was 1.85 ps. The corresponding parameters are gathered in Table 1 where all the settings but σ_t result from the aforementioned optimization and the emittances correspond to

* The work of M.R. and P.P. is supported by the US Department of Energy under Contract DE-FG02-08ER41532 with Northern Illinois University. W.G. and J.P. are supported by the U.S. Department of Energy under Contract No. DE-AC02-06CH11357 with Argonne National Laboratory. D. M is supported by the Department of Education under contract P116Z010035 with Northern Illinois University

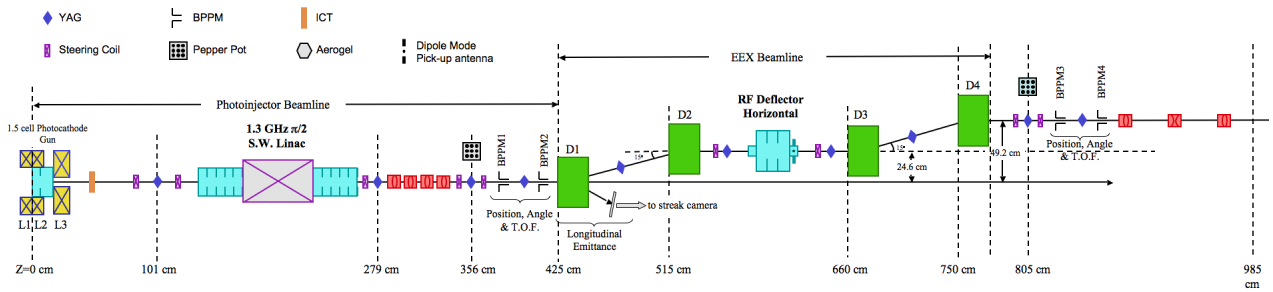

Figure 1: Layout of the emittance exchange proof-of-principle experiment at the AWA. The green and red rectangles respectively correspond to dipoles and quadrupoles magnets. The labels L1, L2, L3 indicates the locations of the three solenoids around the gun. The locations of planned transverse and longitudinal emittance diagnostics are also shown.

the experimentally achieved value of $\sigma_t \simeq 1.9$ ps.

MEASUREMENTS

The purpose of the series of experiments reported below was to confirm the parameters simulated with ASTRA for a laser pulse duration $\sigma_t = 1.9$ ps. The required laser spot size of 4 mm (rms) is significantly larger than the nominal one and we presently observe significant intensity non-uniformities across the area of the uv laser. These non-uniformities have significant impact on the transverse and longitudinal emittance produced by the rf gun.

The parameters resulting from the numerical optimization of the beamline were used as initial settings for the AWA beamline and were then slightly altered to match experiment with simulations. n particular the simulated beam energy and evolution of the transverse envelop shown in Fig. 2 were experimentally reproduced.

The transverse emittance was measured using a standard quadrupole scan technique [5]. Simulations of the method with IMPACT-T [4] support the use of a fitting algorithm that does not include linear space charge force to infer the emittance values. The squared beam size dependence on the quadrupole magnetic strength k is parametrized by a second-order polynomial $\sigma^2 = Ak^2+Bk+C$ and the emittance is estimated as $\varepsilon = [4AC - B^2]^{1/2}/(2D^2)$. Fig. 3 shows the measured squared beam size as a function of k along with the corresponding quadratic fit. The inferred emittance values are in good agreement with the one predicted by ASTRA; see Table 1.

The longitudinal emittance is measured by scanning the booster phase and measuring the resulting energy spread. A fitting technique similar to the one used in the quadrupole scan method provides the longitudinal emittance; see e.g. Ref [8]. Because of the low energies (few MeV) reached during the phase scan, the longitudinal transport matrix [in

Symbol (unit)	ASTRA	Experiment
Q (pC)	100	100 ± 10
laser σ_t (ps)	1.95	1.85 ± 0.2
rms laser size (mm)	4.0	4.0
gun field (MV/m)	43.92	47 ± 2
gun phase (deg.)	65	60 ± 5
booster field (MV/m)	15.75	15.5 ± 1
booster phase (deg.)	50.35	52 ± 4
L1 peak B-field (T)	0.062	0.0618 ± 0.0031
L2 peak B-field (T)	-0.062	-0.0626 ± 0.003
L3 peak B-field (T)	-0.228	-0.228 ± 0.0114
ε_x (μm)	19.5	18.5 ± 2
ε_y (μm)	19.5	21.2 ± 2
ε_z (μm)	7.40	-

Table 1: Optimized settings and beam parameters at $z = 2.79$ m using ASTRA and corresponding experimental values. The value of σ_t was the one experimentally achieved.

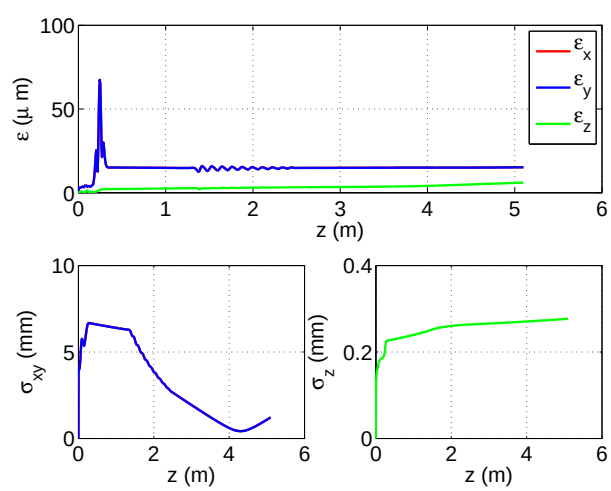

Figure 2: Top plot is the transverse emittance (blue and red) and longitudinal emittance evolution along AWA beam line. Bottom plot is for the beam size and bunch length evolution.

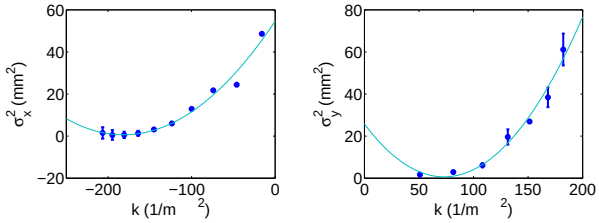

Figure 3: Squared horizontal (left) and vertical (right) beam sizes versus quadrupole magnetic strength. The data (blue circles) and corresponding quadratic fit (green lines) are shown. Emittance values inferred from the quadratic fit are $\varepsilon_x = 18.5 \pm 2$ μm and $\varepsilon_y = 16.2 \pm 2$ μm.

(z, δ) phase space] of the booster was modeled as a series of thin-lens cavity matrix interleaved by drift spaces of length L with longitudinal dispersion $R_{56} = -L/\gamma^2(z)$ where $\gamma(z)$. the Lorentz factor, varies as the beam propagates through the booster. We verified the thereby devised semi-analytical model for the transfer matrix is in agreement with the one numerically evaluated from particle tracking simulations; see Fig. 4.

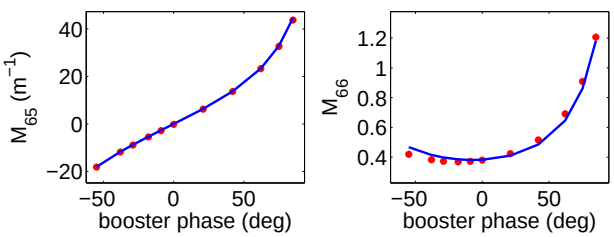

Figure 4: M_{65} (left) and M_{66} (right) element of the transfer matrix of the booster cavity in the longitudinal phase space (z, δ). The simulated transfer matrix using IMPACT-T (red symbols) is compared with analytical calculation (blue lines).

The energy spread is measured downstream of a vertically-bending spectrometer, located $\simeq$ 2 m downstream of the booster, where the vertical dispersion is $|\eta_y| \simeq 18$ cm. An horizontal slit located upstream of the dipole, is imaged onto the YAG screen to improve the energy spread measurement resolution. Fig. 5 shows the evolution of beam's mean and rms momentum as a function of the booster phase. The data are consistent with numerical simulations with ~ 8 μm longitudinal emittance.

FUTURE PLANS & SUMMARY

Although the transverse emittances measured are in good agreement with the predicted one, the longitudinal emittance measurement needs to be refined. We have tested a maximum-entropy-based tomography algorithm [9] using simulated data (see Fig. 6) and plan on using this algorithm to measure the longitudinal emittance.

On the experimental side several improvements are

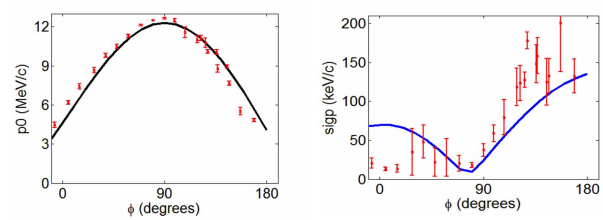

Figure 5: Mean (left) and rms (right) momentum versus booster phase. Red symbols are measurement and solid line are simulations with $\varepsilon_z \simeq 8$ μm.

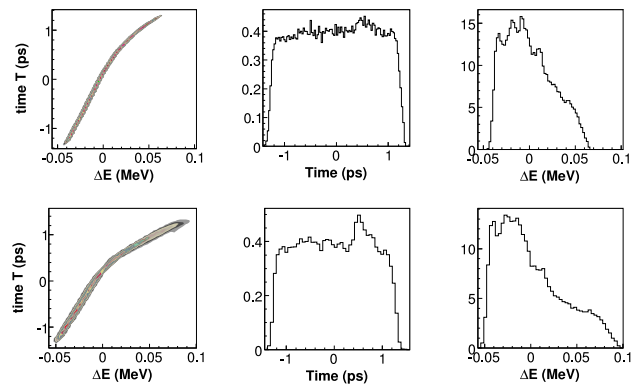

Figure 6: Simulation of longitudinal phase space reconstruction via a maximum-entropy-based tomographic algorithm. The top row shows the initial simulated longitudinal phase space (right column), and associated temporal (middle) and energy (left) projections. The bottom row displays same data tomographically reconstructed after simulation of the booster phase scan.

needed. In particular the photocathode laser transverse uniformity requires further work and the observed significant phase jitter need to be addressed. Nevertheless the preliminary measurements presented in this Paper indicate that AWA can operate with an emittance partition provding a transverse emittance more than twice the longitudinal emittance.

REFERENCES

[1] See `http://gate.hep.anl.gov/awa` .

[2] M. Borland and H. Shang, `geneticOptimizer`, private communication.

[3] K. Flöttmann, ASTRA a space charge tracking algorithm available at `http://www.desy.de/~mpyflo/` .

[4] J. Qiang, *et al.*, *Phys. Rev. STAB* **9**, 044204 (2006).

[5] J. Rees and L. Rvikin, report SLAC-PUB-3305 (1984).

[6] M. G. Minty and F. Zimmermann, *Measurement and Control of Charged Particle Beams*, Springer (2003).

[7] M. Rihaoui, et al., these proceedings.

[8] T. Shaftan, et al, in Proc. EPAC02 (Paris), 834 (2002).

[9] N. V. Denisova, *J. Phys. D: Appl. Phys.* **31**, 1888 (1998).